

## Impact of Sea Spray on Air–Sea Fluxes. Part II: Feedback Effects

JAMES A. MUELLER AND FABRICE VERON

*School of Marine Science and Policy, University of Delaware, Newark, Delaware*

(Manuscript received 1 November 2013, in final form 4 August 2014)

### ABSTRACT

This paper presents estimations for the transfer of momentum, heat, and water mass between the air and the sea. The results from Lagrangian stochastic simulations of sea spray drops (see Part I), along with two sea spray generation functions, are used to calculate the spray-mediated flux components of the air–sea fluxes. When the spray-mediated fluxes constitute a significant fraction of the total fluxes under certain conditions, their feedback effect on the atmosphere cannot be neglected. The authors derive a simplified feedback model to investigate such cases, finding that the spray-mediated fluxes may be especially sensitive to the size distribution of the drops. The total effective air–sea fluxes lead to drag and enthalpy coefficients that increase modestly with wind speed. The rate of increase for the drag coefficient is greatest at moderate wind speeds, while the rate of increase for the enthalpy coefficient is greatest at higher wind speeds where the spray is ubiquitous.

### 1. Introduction

Numerous theoretical studies concerning the role of spray in high wind speed conditions have supplemented microphysical and transport models like that in [Mueller and Veron \(2014, hereinafter Part I\)](#). Expanding upon the work of Sir James Lighthill, [Barenblatt et al. \(2005\)](#) developed a flow model from the sandwich model of tropical cyclones. In Lighthill's sandwich model ([Lighthill 1999](#)), spray forms a layer that can be conceptualized as a third fluid, sandwiched between the sea and air, acting as a lubrication layer that ultimately decreases the surface drag on the airflow. Relatedly, some studies have investigated the stability effects of the layer of drops (e.g., [Bye and Jenkins 2006](#); [Kudryavtsev 2006](#); [Kudryavtsev and Makin 2011](#); [Bao et al. 2011](#)). Essentially, a droplet-laden flow near the surface forms a stably stratified layer that dampens the turbulent mixing and its corresponding energy dissipation—and thus, the drag on the flow for any given wind speed. [Richter and Sullivan \(2013\)](#), however, found that the inertial impacts of sea spray dominate its stability effects.

In addition to the potential reduction of the surface drag, [Andreas and Emanuel \(2001\)](#) suggested that

reentrant spray enhances the enthalpy flux, although the reentrant spray could have a damping effect on the wave-induced stress at high wind speeds too. [Andreas \(2004\)](#) further postulated that the effective stress at high wind speeds could also be reduced by the vertical redistribution of momentum from reentering spray. All of these possibilities, if realized, would increase the ratio of the effective enthalpy and drag transfer coefficients ( $C_K$  and  $C_D$ , respectively).

[Emanuel \(1986\)](#) showed that numerically simulated hurricanes could not sustain hurricane-strength winds if parameterizations for  $C_D$  and  $C_K$  that were derived from observations in low-to-moderate winds were simply extrapolated to high winds. Subsequently, [Emanuel \(1995\)](#) bracketed the  $C_K/C_D$  ratio necessary for producing realistic modeled hurricanes between 0.75 and 1.5, values much higher than extrapolated parameterizations would predict. To satisfy this 0.75 threshold, at least one of the following must be true at high wind speeds: the enthalpy transfer coefficient is greater than the extrapolated value or the momentum transfer coefficient is less than the extrapolated value. Recent studies (e.g., [Haus et al. 2010](#); [Bryan and Rotunno 2009a,b](#)) have scrutinized the 0.75 threshold more closely, and its validity or application remains an open question. Recent data (e.g., [Black et al. 2007](#); [Drennan et al. 2007](#); [French et al. 2007](#); [Zhang et al. 2008](#)) suggest it may not be a constraining limit as assumed in some previous studies. Nevertheless, sea spray

---

*Corresponding author address:* Fabrice Veron, University of Delaware, 112C Robinson Hall, Newark, DE 19716.  
E-mail: fveron@udel.edu

offers a logical, potential candidate for both possibilities of increased enthalpy transfer or reduced drag.

## 2. Similarity theory

In a fully developed turbulent boundary layer found commonly in the marine atmospheric boundary layer (MABL), the structure of the turbulent flow in the surface layer is determined by mechanical and buoyant (thermal) forces. Obukhov (1946) assumed, according to Buckingham's II theorem, that there is only one parameter with the dimension of length that incorporates the physical variables (buoyancy parameter, momentum flux scale or friction velocity, and surface buoyancy flux) relevant to turbulence in the surface layer. Obukhov (1946) and Monin and Obukhov (1954) were the first to develop a similarity hypothesis regarding the statistical nature of the turbulent flow dependent on the relative forcing of the mechanical and buoyant mechanisms. Although Monin–Obukhov (M–O) similarity theory was originally applied to dry air, it has since been extended to moist air such that the structure of turbulence is determined by the height above the surface  $z$ , the buoyancy parameter  $g/\Theta_v$ , the momentum flux scale or friction velocity  $u_*$ , and the surface buoyancy flux  $B_p$ , with the acceleration of gravity  $g$  and virtual potential temperature  $\Theta_v$ . In traditional boundary layer flow, the last two parameters are defined by the surface fluxes:

$$u_* = \left[ \frac{|\tau(0)|}{\rho} \right]^{1/2}, \quad (1)$$

$$B_p = \frac{-H(0)}{\rho c_p} [1 + 0.6078Q(0)] + 0.6078\Theta(0) \frac{-M(0)}{\rho}, \quad (2)$$

where  $\rho$  and  $c_p$  are the density and specific heat of air, respectively;  $\tau(0)$ ,  $H(0)$ , and  $M(0)$  are, respectively, the momentum, sensible heat, and water vapor fluxes at the surface; and  $Q(0)$  and  $\Theta(0)$  are the specific humidity and potential temperature at the surface. Note that the sensible heat and water vapor fluxes (and consequently the latent heat flux) are defined as positive into the boundary (the sea in this case) to be consistent with the sign convention of the momentum flux. As mentioned previously, the Obukhov length is fully defined from those physical variables:

$$L = \frac{\Theta_v u_*^3}{\kappa g B_p}, \quad (3)$$

where  $\kappa$  is the von Kármán constant, taken to be 0.4 here.

We follow the standard Reynolds decomposition of the instantaneous velocity  $u_i$ , potential temperature  $\theta$ , and specific humidity  $q$  of the air:

$$\begin{aligned} u_i &= U_i + u'_i, \\ \theta &= \Theta + \theta', \\ q &= Q + q'. \end{aligned} \quad (4)$$

Here,  $U_i$ ,  $\Theta$ , and  $Q$  are the ensemble (or temporal) averages in surface-following coordinates and  $u'_i$ ,  $\theta'$ , and  $q'$  are the turbulent deviations from the respective means. We only consider the streamwise horizontal and vertical directions,  $i = \{1, 3\}$ .

According to M–O similarity theory, the terms in the turbulent kinetic energy (TKE) budget become universal functions of  $z/L$  when normalized by  $\kappa z/u_*^3$ . This includes the mechanical production of turbulence term ( $-u'_1 u'_3 \partial U_1 / \partial z$ ) from shear:

$$\phi_m(z/L) = \frac{\kappa z}{u_*} \frac{\partial U_1}{\partial z}, \quad (5)$$

where  $\phi_m$  is the universal, dimensionless shear, and  $U_1$  is the mean wind aligned with the direction of the mean flow. Sufficiently far away from the surface to be outside the viscous sublayer, the turbulent flux  $\overline{u'_1 u'_3}$  is equal to  $-u_* |u_*|$ .

Like the TKE budget, the terms in the scalar variance budgets become universal functions of  $z/L$  when normalized by  $(-\kappa z/\chi_*) (\partial \chi / \partial z)$ , where  $\chi_* = \{\theta_*, q_*\}$  are the corresponding flux scales. Consequently, the terms in the potential temperature and specific humidity variance budgets reduce to universal functions, including the production of turbulence terms from gradients in the mean profiles of potential temperature ( $-\overline{\theta' u'_3} \partial \Theta / \partial z$ ) and specific humidity ( $-\overline{q' u'_3} \partial Q / \partial z$ ):

$$\phi_\theta(z/L) = \frac{\kappa z}{\theta_*} \frac{\partial \Theta}{\partial z}, \quad \text{and} \quad (6)$$

$$\phi_q(z/L) = \frac{\kappa z}{q_*} \frac{\partial Q}{\partial z}, \quad (7)$$

where  $\phi_\theta$  and  $\phi_q$  are the universal, dimensionless gradients for potential temperature and specific humidity, respectively. Sufficiently far away from the surface to be outside the molecular sublayers, the turbulent fluxes  $\overline{\theta' u'_3}$  and  $\overline{q' u'_3}$  are equal to  $-\theta_* |u_*|$  and  $-q_* |u_*|$ , respectively;  $\theta_*$  is the heat flux scale, and  $q_*$  is the water mass flux scale. As in Part I, we note the sign convention with which positive fluxes are into the ocean and negative fluxes are out of the ocean and into the atmosphere.

A basic assumption of M–O similarity theory is that the fluxes are constant with height within the surface layer. Data suggest this assumption provides a good approximation for the MABL at low-to-moderate wind speeds (Edson and Fairall 1998). Its applicability for high wind regimes remains an open question, however. Further details of M–O similarity theory can be found in countless texts (e.g., Lumley and Panofsky 1964; Wyngaard 1973).

### 3. Model description

The distinct pathways through which the ocean and atmosphere interact are the air–sea interface itself, entrained bubbles, and airborne drops. As many previous studies have suggested (e.g., Andreas 2011, and citations therein), the air–sea interface and air–sea spray interface constitute nearly all of the total air–sea fluxes considered here. Accordingly, we explicitly assume the total momentum, sensible heat, and water mass fluxes can be decomposed into air–sea interfacial and spray-mediated components as follows:

$$\tau = \tau_{\text{int}} + \tau_{\text{sp}}, \quad (8)$$

$$H = H_{\text{int}} + \alpha H_{\text{sp}} - \beta E_{\text{sp}}, \quad \text{and} \quad (9)$$

$$M = M_{\text{int}} + \beta M_{\text{sp}}, \quad (10)$$

where the subscripts int and sp denote the air–sea interfacial and spray-mediated components, respectively. The latent heat flux  $E$  and individual components  $E_{\text{int}}$  and  $E_{\text{sp}}$  can be found by multiplying the respective water mass flux by the latent heat of vaporization  $L_v$ . The energy necessary to evaporate the droplets must be extracted from the sensible heat in the near-surface atmosphere, and consequently the spray latent heat flux  $E_{\text{sp}}$  must also appear in the sensible heat flux balance. The variables  $\alpha$  and  $\beta$  are feedback coefficients that increase or decrease the efficiency of the spray-mediated heat and water mass fluxes due to changes in atmospheric conditions from the spray-mediated fluxes. They are equal to one in the absence of feedback.

#### a. Fluxes at the air–sea interface

The momentum flux at the surface can be further decomposed into viscous (or tangential), wave-induced, and separation stress components:

$$\tau_{\text{int}}|_{z=0} = \tau_\nu + \tau_w + \tau_s, \quad (11)$$

where  $\tau_\nu$ ,  $\tau_w$ , and  $\tau_s$  are the viscous, wave-induced, and separation stresses, respectively, and  $z$  is the height above the wavy interface. The surface stresses without feedback

effects from the spray-mediated fluxes are modeled according to Mueller and Veron (2009b, 2010b).

The sensible heat and water mass fluxes at the interface are decomposed into molecular and nonmolecular components:

$$H_{\text{int}}|_{z=0} = H_{\text{mol}} + H_{\text{nm}}, \quad \text{and} \quad (12)$$

$$M_{\text{int}}|_{z=0} = M_{\text{mol}} + M_{\text{nm}}, \quad (13)$$

where the subscripts mol and nm designate the molecular and nonmolecular components, respectively. These surface fluxes without feedback effects from the spray-mediated fluxes are modeled according to Mueller and Veron (2010b). The nonmolecular components include wave effects such as airflow separation (Mueller and Veron 2010b).

#### b. Fluxes at the air spray interface

The spray-mediated momentum flux can be expressed as

$$\begin{aligned} \tau_{\text{sp}} &= \int \frac{4}{3} \pi (\rho_{p,f} v_{1,f} r_f^3 - \rho_{p,0} v_{1,0} r_0^3) \frac{dF}{dr_0} dr_0, \\ &= \int \Delta \tau_{\text{sp}}(r_0) \frac{dF}{dr_0} dr_0 \\ &= \int d\tau_{\text{sp}}(r_0), \end{aligned} \quad (14)$$

where  $\Delta \tau_{\text{sp}}$  is the mean exchange of momentum for each drop radius (see Part I);  $\rho_p$ ,  $v_1$ , and  $r$  are the drop density, horizontal velocity, and radius, respectively; the subscripts  $f$  and  $0$  designate the final and initial values, respectively; and  $dF/dr_0$  is the sea spray generation function (SSGF)—the number of drops formed per square meter of ocean surface per second per micrometer increment of drop radius. Here, we consider the radius at the formation of the drop  $r_0$ .

The spray-mediated sensible and latent heat fluxes can be expressed, respectively, as

$$\begin{aligned} H_{\text{sp}} &= \int \frac{4}{3} \pi (\rho_{p,f} c_{\text{ps},f} T_{p,f} r_f^3 - \rho_{p,0} c_{\text{ps},0} T_{p,0} r_0^3) \frac{dF}{dr_0} dr_0, \\ &= \int \Delta H_{\text{sp}}(r_0) \frac{dF}{dr_0} dr_0 \\ &= \int dH_{\text{sp}}(r_0), \quad \text{and} \end{aligned} \quad (15)$$

$$\begin{aligned} E_{\text{sp}} &= \int \frac{4}{3} \pi (\rho_{p,f} L_{v,f} r_f^3 - \rho_{p,0} L_{v,0} r_0^3) \frac{dF}{dr_0} dr_0, \\ &= \int \Delta E_{\text{sp}}(r_0) \frac{dF}{dr_0} dr_0 \\ &= \int dE_{\text{sp}}(r_0), \end{aligned} \quad (16)$$

where  $\Delta H_{\text{sp}}$  and  $\Delta E_{\text{sp}}$  are the mean exchanges of sensible and latent heat, respectively, for each drop radius obtained in Part I;  $c_{\text{ps}}$  and  $T_p$  are, respectively, the specific heat and temperature of the saline, sea spray drop. Again, the spray-mediated latent heat flux  $E_{\text{sp}}$  is related to the spray-mediated water mass flux  $M_{\text{sp}}$  by the latent heat of vaporization  $L_v$ . We note that both the specific heat and the latent heat of vaporization depend on the local drop conditions.

### c. Sea spray generation function

The uncertainties of both the amount and size distribution of sea spray generated at the surface, that is, the sea spray generation function, continue to obscure spray-mediated momentum and scalar fluxes, especially in intense wind conditions (Veron et al. 2012). Most previous studies assume a constant form, or spectral shape, for the droplet distribution that is then scaled with wind forcing. We use two different SSGFs for comparison. Through the distinction between the drops formed at the surface and the drops transported vertically where measurements are routinely made, we implement a recent spume generation function, hereinafter referred to as the Mueller–Veron SSGF (Mueller and Veron 2009c). Unlike most previous studies, both its spectral form and magnitude change with wind forcing. For comparison, we consider another SSGF that has been used in many other sea spray studies, the generation function from Fairall et al. (1994) (also reported in Andreas 2002). While the magnitude of this SSGF changes with wind forcing, its spectral shape does not.

#### 1) MUELLER–VERON SSGF

The Mueller–Veron SSGF has two important advantages: its wind forcing dependence is based on the total stress in the boundary layer rather than the 10-m wind speed, and both its magnitude and spectral shape change with wind forcing. Intuitively, the peak radius of the size distribution becomes smaller with increased wind forcing, as expected from the increasing turbulent kinetic energy extending to smaller and smaller scales. Various theoretical models for droplet distributions in a turbulent carrier fluid (e.g., Hinze 1955) support such an expectation, for which the mean radius reduces with wind speed.

The Mueller–Veron SSGF model assumes a similar mechanism for the generation and breakup of spume drops as that found in experiments of round water jets. It converts the relevant parameters from those experiments to bulk air–sea variables, providing the drop distribution for each drop formation event. With the length of breaking wave crests per unit area per unit time from

the wave model embedded in the air–sea stress calculation, it also scales the spectral shape with the number of breakup event occurrences at the air–sea interface, providing the appropriate magnitude. In bulk variables, it reduces to

$$\frac{dF}{dr_0} = \frac{2.935 \times 10^{-6} (\Delta U_1)^2 \nu^2}{u_*^4 \int p(\hat{r}_0) r_0^3 dr_0} \times \left( \frac{\rho^2 \nu |\Delta U_1|^3}{\rho_p \sigma_0 u_*^2} \right)^{1/3} L_{\text{br}} p(\hat{r}_0), \quad (17)$$

where  $\Delta U_1 = U_1(10) - U_1(0)$  is the difference in the bulk, streamwise velocities of the fluid phases, which Mueller and Veron (2009c) assumed to be the difference in the 10-m and surface velocities;  $\sigma_0$  is the surface tension at the air–sea interface;  $\nu$  is the kinematic viscosity of air;  $\rho_p$  is the density of the drop;  $L_{\text{br}}$  is the total length of breaking wave crests per unit area per unit time;  $\hat{r}_0 = r_0/\bar{r}_0$  is the normalized drop radius; and  $\bar{r}_0 = 0.8668 \times 10^6 \nu \Delta U_1 / u_*^2$  is the mean volume equivalent radius in micrometers. The probability distribution function follows the gamma distribution with a mean of 1 and variance of  $n^{-1}$ , defined as

$$p(\hat{r}_0) = n^n \hat{r}_0^{n-1} e^{-n\hat{r}_0} / \Gamma(n), \quad (18)$$

with inverse variance

$$n = 183.2 \left[ \frac{\rho^2 (\Delta U_1)^2 \bar{r}_0}{\rho_p \sigma_0} \right] + 2. \quad (19)$$

#### 2) FAIRALL ET AL. (1994) SSGF

Andreas (2002) reviewed an extensive list of SSGFs available in the literature and recommended the SSGF found in Fairall et al. (1994). The Fairall et al. (1994) SSGF,  $dF_F/dr_0$ , is the Andreas (1992) SSGF,  $dF_{A92}/dr_0$ , at  $11 \text{ m s}^{-1}$  normalized by the whitecap B coverage at  $11 \text{ m s}^{-1}$  wind speed and scaled by the whitecap coverage at any given wind speed:

$$\frac{dF_F}{dr_0} = \frac{W_B[U_1(10)]}{W_B(11)} \frac{dF_{A92}}{dr_0} \Big|_{U_1(10)=11 \text{ m s}^{-1}}, \quad (20)$$

where function  $W_B = 3.8 \times 10^{-6} U_1(10)^{3.4}$  is the whitecap B coverage from Monahan and O’Muircheartaigh (1980).

The Andreas (1992) SSGF was originally reported in terms of the equilibrium radius at 80% humidity  $r_{80}$ :

$$\log\left(\frac{dF_{A92}}{dr_{80}}\right) = B_0 + B_1[\log(r_{80})] + B_2[\log(r_{80})]^2 + B_3[\log(r_{80})]^3 + B_4[\log(r_{80})]^4$$

for  $0.8 \leq r_{80} < 15 \mu\text{m}$

$$\frac{dF_{A92}}{dr_{80}} = C_1 r_{80}^{-1} \quad \text{for } 15 \leq r_{80} < 37.5 \mu\text{m}$$

$$\frac{dF_{A92}}{dr_{80}} = C_2 r_{80}^{-2.8} \quad \text{for } 37.5 \leq r_{80} < 100 \mu\text{m}$$

$$\frac{dF_{A92}}{dr_{80}} = C_3 r_{80}^{-8} \quad \text{for } 100 \leq r_{80} < 250 \mu\text{m}, \quad (21)$$

where  $B_0 = 4.405$ ,  $B_1 = -2.646$ ,  $B_2 = -3.156$ ,  $B_3 = 8.902$ ,  $B_4 = -4.482$ ,  $C_1 = 1.02 \times 10^4$ ,  $C_2 = 6.95 \times 10^6$ , and  $C_3 = 1.75 \times 10^{17}$  at  $11 \text{ m s}^{-1}$  wind speed. To convert this function to the initial radius at formation, we assume the standard, simple relationships derived from [Fitzgerald \(1975\)](#):

$$r_{80} = 0.518 r_0^{0.976}, \quad (22)$$

$$\frac{dF_{A92}}{dr_0} = \frac{dF_{A92}}{dr_{80}} \frac{dr_{80}}{dr_0}, \quad (23)$$

and

$$\frac{dr_{80}}{dr_0} = 0.506 r_0^{-0.024}. \quad (24)$$

#### d. Fluxes above sea spray layer

According to the M–O similarity theory summarized in [section 2](#), the total fluxes are constant with height. If the theory holds in the MABL with sea spray present, Eqs. (5)–(7) imply a velocity, potential temperature, and specific humidity gradient just above the wave boundary layer and sea spray layer:

$$\frac{\partial U_1}{\partial z} = \frac{u_*}{\kappa z} \phi_m\left(\frac{z}{L}\right), \quad (25)$$

$$\frac{\partial \Theta}{\partial z} = \frac{\theta_*}{\kappa z} \phi_\theta\left(\frac{z}{L}\right), \quad \text{and} \quad (26)$$

$$\frac{\partial Q}{\partial z} = \frac{q_*}{\kappa z} \phi_q\left(\frac{z}{L}\right), \quad (27)$$

where we assume that the turbulent flux components account for the total flux just above the wave boundary and sea spray layers such that

$$u_* |u_*| = \tau/\rho = -\overline{u_1' u_3'}, \quad (28)$$

$$\theta_* |u_*| = H/\rho c_p = -\overline{\theta' u_3'}, \quad \text{and} \quad (29)$$

$$q_* |u_*| = M/\rho = -\overline{q' u_3'}. \quad (30)$$

Upon integration of Eqs. (25)–(27), we recover the standard log layers:

$$U_1(z) - U_1(0) = \frac{u_*}{\kappa} \left[ \log\left(\frac{z}{z_0}\right) - \Psi_m\left(\frac{z}{L}\right) \right], \quad (31)$$

$$\Theta(z) - \Theta(0) = \frac{\theta_*}{\kappa} \left[ \log\left(\frac{z}{z_\theta}\right) - \Psi_\theta\left(\frac{z}{L}\right) \right], \quad \text{and} \quad (32)$$

$$Q(z) - Q(0) = \frac{q_*}{\kappa} \left[ \log\left(\frac{z}{z_q}\right) - \Psi_q\left(\frac{z}{L}\right) \right]. \quad (33)$$

The terms  $\Psi_m(z/L)$ ,  $\Psi_\theta(z/L)$ , and  $\Psi_q(z/L)$  are the adjustments of the profiles due to the relative contributions of mechanical and buoyancy forcing at height  $z$  in the boundary layer;  $z_0$ ,  $z_\theta$ , and  $z_q$  are the algebraically manipulated integration constants commonly referred as the roughness lengths. As in [Part I](#), these integration constants are iterated upon in the model from specified profile forms and boundary conditions.

Although this result may, at first, seem surprising, the wave boundary and sea spray layers are analogous to the viscous sublayer. Near the surface, both contribute significant fractions (if not 100% combined) of the total stress; yet, above the layers, the turbulent stress accounts for nearly all of the total stress. Indeed, [Mueller and Veron \(2009b\)](#) and [Kudryavtsev and Makin \(2007\)](#) suggest that the steep, capillary waves carry a significant portion of the wave-induced stress, which dissipates rapidly with distance away from the surface. Likewise, the spray-mediated fluxes presumably dissipate rapidly with distance away from the surface. Such a presumption is justified not only from the mean height of the sea spray drops, which are shown in the results of [Part I](#), but also the relative gradients of the mean profiles with height. Essentially, the exchanges happen more rapidly near the surface due to stronger gradients in the ambient conditions. Nevertheless, caution should be given to such an application of M–O similarity theory. This application certainly raises questions about the validity of the constant flux assumption and the extension of a theory originally formulated for mechanical and thermal forcing only. Recently, [Bianco et al. \(2011\)](#) assumed a variable total heat flux in the near-surface layer due to the presence (and evaporation) of sea spray drops. Though not conclusive, their results suggest that a displacement value, equal to the mean wave height, may need to be included in the logarithmic profiles to

maintain the validity of the constant flux assumption. As discussed in more detail in [Part I](#), our model uses wave-following coordinates and includes a term in the logarithmic profiles that represents a displacement value.

### e. Profiles of the flux components

With the fluxes at the surface and above sea spray layer well defined, the transition between these two limits, and within the sea spray layer, needs to be explored further. While [Mueller and Veron \(2009a, 2010a\)](#) described the profiles of the flux components, excluding the spray-mediated fluxes, in detail, we consider the following turbulent stress profile for the purpose of this study:

$$\tau_t(z) = \tau(0) - \tau_v(z) - \tau_w(z) - \tau_{sp}(z), \quad (34)$$

where  $\tau_t = -\overline{\rho u'_1 u'_3}$  is the local turbulent stress. The turbulent component is defined such that the total stress is constant with height, in accordance with M-O similarity theory.

The vertical profile of the viscous stress is defined from the horizontal velocity gradient:

$$\tau_v(z) = \rho\nu \frac{\partial U_1(z)}{\partial z}. \quad (35)$$

Similar to [Makin and Kudryavtsev \(1999\)](#) and [Mueller and Veron \(2009a\)](#), the wave-induced stress profile is taken to be

$$\tau_w(z) = \int d\tau_w(k) \cos(5\pi kz) \exp(-10kz), \quad (36)$$

where  $d\tau_w(k)$  is the wave-induced stress at the surface for each wavenumber.

[Andreas \(2004\)](#) extends, by analogy, the speculative concentration profile from [Andreas and DeCosmo \(1999\)](#) to define the spray-mediated stress profile:

$$\tau_{sp}(z) = \tau_{sp}(0) \exp(-z/A), \quad (37)$$

where [Andreas \(2004\)](#) took  $A = -2A_{1/3}/\ln(0.001)$  with significant wave amplitude,  $A_{1/3} = 0.0015U_1(10)^2$ . We take  $A(r)$  to be the mean, maximum height for each drop radius from the stochastic simulations of [Part I](#):

$$\tau_{sp}(z) = \int d\tau_{sp}(0, r_0) \exp[-z/A(r_0)], \quad (38)$$

where  $d\tau_{sp}(0, r_0)$  is the spray-mediated stress for each radius.

Similar to the momentum flux, the constant flux assumption yields the turbulent sensible heat and water mass flux profiles,

$$H_t(z) = H(0) - H_{mol}(z) - [\alpha H_{sp}(z) - \beta E_{sp}(z)], \quad \text{and} \quad (39)$$

$$M_t(z) = M(0) - M_{mol}(z) - \beta M_{sp}(z), \quad (40)$$

and the turbulent latent heat flux is  $E_t(z) = L_v M_t$ . The molecular fluxes are defined from the profile gradients:

$$H_{mol}(z) = \rho c_p \kappa_\theta \frac{\partial \Theta(z)}{\partial z}, \quad \text{and} \quad (41)$$

$$M_{mol}(z) = \rho \epsilon \frac{\partial Q(z)}{\partial z}, \quad (42)$$

where  $\kappa_\theta$  and  $\epsilon$  are the diffusivities of heat and water vapor, respectively.

The spray-mediated sensible heat and water mass profiles take a similar form as the spray-mediated stress profile:

$$H_{sp}(z) = \int dH_{sp}(0, r_0) \exp[-z/A(r_0)], \quad \text{and} \quad (43)$$

$$M_{sp}(z) = \int dM_{sp}(0, r_0) \exp[-z/A(r_0)], \quad (44)$$

where  $dH_{sp}(0, r_0)$  and  $dM_{sp}(0, r_0)$  are the spray-mediated sensible heat and mass fluxes, respectively, for each radius.

### f. Feedback

The effects of sea spray on the profiles of velocity, potential temperature, and specific humidity are the focus of this subsection. Although included in the model, the effects of the molecular and wave-induced fluxes on the profiles will be excluded here for a clearer presentation of the spray-mediated feedback effects. Rearranging Eq. (5), with a nonsingular vertical coordinate ( $\zeta = z + z_0$ ), the velocity gradient in the sea spray layer is

$$\begin{aligned} \frac{\partial U_1(\zeta)}{\partial \zeta} &= \frac{[\tau_t(\zeta)/\rho]^{1/2}}{\kappa \zeta} \phi_m \\ &= \frac{\tau - \tau_{sp}(\zeta)}{\rho \kappa \zeta \{[\tau - \tau_{sp}(\zeta)]/\rho\}^{1/2}} \phi_m. \end{aligned} \quad (45)$$

We assume the spray stress term is a small fraction of the total stress, as found in [Part I](#), such that to a first-order approximation

$$\frac{\partial U_1(\zeta)}{\partial \zeta} = \frac{u_*}{\kappa \zeta} - \frac{\tau_{sp}(\zeta)}{2\rho \kappa u_* \zeta} \phi_m - \frac{u_*(1 - \phi_m)}{\kappa \zeta}. \quad (46)$$

Note that [Andreas \(2004\)](#) arrived at a similar result using an alternate derivation. The integration of the velocity gradient yields the velocity profile:

$$U_1(\zeta) - U_1(0) = \frac{u_*}{\kappa} \left( \log \frac{\zeta}{z_0} - \Psi_m \right) - \int \frac{d\tau_{\text{sp}}(0, r_0)}{2\rho\kappa u_* A(r_0)} \\ \times \left\{ \text{expint} \left[ \frac{-z_0}{A(r_0)} \right] - \text{expint} \left[ \frac{-\zeta}{A(r_0)} \right] \right\}, \quad (47)$$

where  $\text{expint}(z) = \int_z^\infty [\exp(-z')/z'] dz'$  is the exponential integral. Equation (47) has two distinct components: the first term of the RHS is the standard log layer incorporating the total friction velocity, while the second term on the RHS is the spray-mediated component. The cross-term between the spray-mediated stress and the stability function, which we omit for a clearer presentation, is negligible when the spray-mediated stress is a small fraction of the total stress.

The spray-mediated effects on the potential temperature and specific humidity profiles are similar. Excluding the molecular sublayer effects from the derivation for a clearer presentation, and rearranging Eqs. (6)–(7) with a nonsingular vertical coordinate ( $\zeta_\chi = z + z_\chi$ , where  $z_\chi$  are friction lengths; see Part I), the gradients in the sea spray layer can be written as

$$\frac{\partial \Theta(\zeta_\theta)}{\partial \zeta_\theta} = \frac{H_t(\zeta_\theta)}{\rho\kappa c_p u_* \zeta_\theta} \phi_\theta \\ = \frac{H - [\alpha H_{\text{sp}}(\zeta_\theta) - \beta E_{\text{sp}}(\zeta_\theta)]}{\rho\kappa c_p u_* \zeta_\theta} \phi_\theta, \quad \text{and} \quad (48)$$

$$\frac{\partial Q(\zeta_q)}{\partial \zeta_q} = \frac{M_t(\zeta_q)}{\rho\kappa u_* \zeta_q} \phi_q \\ = \frac{M - \beta M_{\text{sp}}(\zeta_q)}{\rho\kappa u_* \zeta_q} \phi_q. \quad (49)$$

It is important to note that unlike in the case of the momentum flux, we do not need to assume the spray-mediated flux terms are a small fraction of the total fluxes here as long as the second-order spray-mediated stratification effects are neglected. The integration of the potential temperature and specific humidity gradients yield the following profiles:

$$\Theta(\zeta_\theta) - \Theta(0) = \frac{\theta_*}{\kappa} \left( \log \frac{\zeta_\theta}{z_\theta} - \Psi_\theta \right) \\ - \left[ \alpha \int \frac{dH_{\text{sp}}(0, r_0)}{\rho\kappa c_p u_* A(r_0)} - \beta \int \frac{dE_{\text{sp}}(0, r_0)}{\rho\kappa c_p u_* A(r_0)} \right] \\ \times \left\{ \text{expint} \left[ \frac{-z_\theta}{A(r_0)} \right] - \text{expint} \left[ \frac{-\zeta_\theta}{A(r_0)} \right] \right\}, \quad \text{and} \quad (50)$$

$$Q(\zeta_q) - Q(0) = \frac{q_*}{\kappa} \left( \log \frac{\zeta_q}{z_q} - \Psi_q \right) - \beta \int \frac{dM_{\text{sp}}(0, r_0)}{\rho\kappa u_* A(r_0)} \\ \times \left\{ \text{expint} \left[ \frac{-z_q}{A(r_0)} \right] - \text{expint} \left[ \frac{-\zeta_q}{A(r_0)} \right] \right\}. \quad (51)$$

### g. Simplified model of coupled fluxes

The natural approach for the implementation of the spray-mediated feedback on the atmosphere would be to run subsequent Lagrangian stochastic simulations with the updated ambient profiles until the spray-mediated fluxes converged. The computational time required for such an approach, however, would be prohibitive. Instead, we make simplifications based on the stochastic simulation results from Part I.

Because the spray-mediated stress is small relative to the total stress ( $\tau_{\text{sp}} \ll \tau$ ) at moderate and high wind speeds for both of the SSGFs considered, we assume that the transport results (e.g., the spray-mediated stress, residence time, and mean height) from the stochastic simulations of Part I are not altered.

The final radius and temperature of the drops are the remaining values needed to estimate the spray-mediated heat and water mass fluxes with feedback. Because we assume the residence times and transport of the drops will not change due to feedback, we assume the relationships found in Part I provide a good estimate for final temperature and radius as feedback effects change the conditions through which the drops traverse. Specifically, Figs. 9 and 10 from Part I suggest that the radius and temperature upon reentry into the ocean can be predicted from the modified mean profiles and transport results, which again are assumed to be unchanged. The change in temperature and final mass both collapse for all wind forcing conditions when normalized by a steady-state evolution with the drops sorted by their terminal velocity relative to the ambient vertical turbulent velocity instead of being sorted by their radius. The simplified feedback model determines the temperature upon impact as

$$T_{p,f}(r) = T_{p,0} + \hat{T}_p [\tilde{T}_p|_{A(r_0)10} - T_{p,0}], \quad (52)$$

where  $\hat{T}_p$  is the ratio of the temperature change of the drop from the stochastic simulations in Part I relative to the temperature change of the drop when exposed to the ambient conditions (without feedback) for the duration of the mean residence time at one-tenth of the mean,

maximum height above the surface;  $\tilde{T}_p$  is the temperature change of the drop when exposed to the ambient conditions (with feedback) for the duration of the mean residence time at one-tenth of the mean, maximum height. Essentially, the change in temperature ratio accounts for the important variables: residence time, location where the drop spends most of its time, and the thermal response time of the drop.

Similarly the simplified feedback model determines the radius upon impact as

$$r_f(r_0) = \hat{r}_0 \tilde{r}_0 |_{A(r_0)/10}, \quad (53)$$

where  $\hat{r}_0$  is the ratio of the impact radius of the drop from the stochastic simulations relative to the impact radius of the drop when exposed to the ambient conditions (without feedback) for the duration of the mean residence time at one-tenth of the mean, maximum height above the surface;  $\tilde{r}_0$  is the impact radius of the drop when exposed to the ambient conditions (with feedback) for the duration of the mean residence time at one-tenth of the mean, maximum height above the surface. Like the temperature change ratio, the radius ratio accounts for the important variables: residence time, location where the drop spends most of its time, and the speed of evaporation/condensation due to the size of the drop.

Of course, these two ratios ( $\hat{T}_p$  and  $\hat{r}_0$ ) may have embedded artifacts from the potential temperature and specific humidity profiles in the original stochastic simulations. This seems unlikely, however, since the same relationship spanned large differences in the wind speed regime in which the very different molecular and wave-induced contributions created “unique,” near-surface profiles for each wind speed. The relevant parameters are also physically intuitive. Nevertheless, only subsequent stochastic simulations, which include the feedback from the spray-mediated fluxes, can validate the extension of these ratios to conditions in which the spray-mediated fluxes account for a significant portion of the total fluxes.

With the drop temperature and radius upon reentry, the other values in Eqs. (15)–(17) can be calculated directly, yielding the mean exchanges of sensible and latent heat for each radius after accounting for feedback. As before, the summation of the spray-mediated sensible heat and mass fluxes with feedback for each radius  $dH_{sp}^*$  and  $dM_{sp}^*$  produces the total spray-mediated sensible heat and mass fluxes with feedback,  $H_{sp}^*$  and  $M_{sp}^*$ , respectively.

The feedback coefficients for the spray-mediated fluxes can be simply calculated as the ratio of fluxes with feedback and without feedback:

$$\alpha = \frac{H_{sp}^*}{H_{sp}}, \quad \text{and} \quad (54)$$

$$\beta = \frac{E_{sp}^*}{E_{sp}}. \quad (55)$$

The model iterates upon these feedback coefficients, modified profiles, and fluxes until convergence. In addition to impacting the spray-mediated fluxes, the fluxes into and out of the ocean are also affected as the spray alters the near-surface layer. The air–sea interfacial fluxes are calculated as in Part I, with specified profile forms and boundary conditions, but now with modified profiles due to spray.

Table 1 summarizes the key features of this model compared to the models of Edson et al. (1996) and that of the Sea Couche Limite Unidimensionnelle Stationnaire d’Embruns (SEACLUSE) model (Van Eijk et al. 2001; Meirink 2002).

#### 4. Results

In this section, we present the results from the model, focusing on the estimated spray-mediated fluxes with and without feedback and the impact on the total air–sea transfer. Throughout this section, both SSGFs from section 3c are used for comparison. The results without feedback use the Lagrangian results for the best-guess scenario described in Part I. Finally, we present the overall air–sea transfer coefficients.

##### a. Fluxes without feedback

One of the assumptions for the feedback model is that the spray-mediated momentum flux is negligible. Figure 1 shows that this is a fair assumption. In Fig. 1a, the momentum fluxes due to spray plateau around  $15 \text{ m s}^{-1}$  with the Mueller–Veron SSGF and are much lower than that found in Andreas (2004) with the Fairall et al. (1994) SSGF. For a direct comparison, we ran the FORTRAN code, mentioned at the end of Andreas et al. (2008; the results are labeled A2008), under the same conditions as this study. Figure 1b shows that the fraction of stress due to spray never exceeds more than a few percent at high wind speeds. We find a rather stark departure from those results, in which spray carried much of the stress at high wind speeds. The difference is largely because small droplets decelerate significantly as they traverse the lower boundary layer before reentry (as shown in Fig. 7a of Part I), as opposed to impacting the surface at a velocity close to that of the wind speed as hypothesized by Andreas (2004).

In contrast, the spray-mediated heat fluxes are significant. Figures 2 and 3 show substantial spray-mediated sensible and latent heat fluxes, respectively. Unlike the results for the momentum where the total flux depends

TABLE 1. Comparison of the features of the present model and that of the [Edson et al. \(1996\)](#) and the SEACLUSE models.

	<a href="#">Edson et al. (1996)</a>	SEACLUSE	Mueller-Veron
Surface temperature	22°C	15°C	20°C
10-m conditions	RH 80%; 20°C	RH 65%–80%; 10°, 15°, and 20°C	RH 85%; 18°C
Bottom boundary	Flat	<i>n</i> th-order Stokes wave	Linear superposition of empirical wave spectrum ( <a href="#">Elfouhaily et al. 1997</a> )
Airflow			
Wave impacts on mean flow and turbulence	No	Yes	Yes
Simulated airflow separation	No	No	Yes, only during initial ejection [Eq. (43), Part I]
Scalar turbulence	No	No	Yes
Initial conditions			
Drop source height	$H_{m0}$ ; ejection heights from <a href="#">Blanchard and Woodcock (1957)</a>	Surface	Near-dominant wave crest; top of viscous layer plus roughness length and drop radius [Eq. (42), Part I]
Initial drop radius range (microns)	2–200	10–250	25–2000
Initial drop salinity (psu)	0	Seawater	34
Initial vertical velocity	0	Velocity necessary for drops to reach observed heights ( <a href="#">Blanchard and Woodcock 1957</a> )	Wave-induced vertical velocity at drop location and vertical component of local airflow
Source function	<a href="#">Andreas (1992)</a>	<a href="#">Andreas (1992)</a>	<a href="#">Fairall et al. (1994)</a> ; <a href="#">Mueller and Veron (2009c)</a>
Drop evolution			
Equation of motion terms	Gravity and drag relation from <a href="#">Clift et al. (1978)</a>	Gravity and drag relation from <a href="#">Raudviki's (1976)</a>	Gravity, drag relation from <a href="#">Clift and Gauvin (1970)</a> , added mass, pressure gradient acceleration, and Basset history [Eq. (35)–(36), Part I]
Ventilation of drops by airflow	Yes	No	Yes
Drop temperature	<a href="#">Pruppacher and Klett (1978)</a>	Simplified to be wet bulb temperature	Modified <a href="#">Andreas (1990)</a> with ventilation coefficient
Drop radius	<a href="#">Beard and Pruppacher (1971)</a> with curvature effects ( <a href="#">Andreas 1989</a> )	<a href="#">Mestayer et al. (1990)</a>	Modified <a href="#">Andreas (1990)</a> with ventilation coefficient
Spray feedback on atmosphere			
Stability effects from total mixed-phased density	No	Yes	No
Spray impacts on atmospheric mean profiles and turbulence	Yes	Profiles only	Yes

primarily on the reentrant spray impact velocity, the exchange of heat is more dependent on residence time and upward transport during which the droplets cool down and evaporate. Consequently, at wind speeds below  $25 \text{ m s}^{-1}$ , the spray-mediated heat fluxes with the [Fairall et al. \(1994\)](#) SSGF track those estimated in A2008 fairly closely. At higher wind speeds, however, the magnitude of the heat fluxes becomes larger than those from A2008. Our results indicate that the spray carries approximately 10% of the total air–sea sensible heat flux at  $10 \text{ m s}^{-1}$  and half of the total sensible heat flux by  $35 \text{ m s}^{-1}$ . With the air

spray, latent heat flux time scale being much longer than that of the sensible heat flux (i.e., it takes longer for droplets to transfer mass than adjust their temperature), the spray comparatively supports a smaller fraction of the total air–sea latent heat flux with a contribution of approximately 30% by  $40 \text{ m s}^{-1}$ .

The fluxes from A2008 represent scaled spray fluxes with coefficients optimized to account for the difference between observations of total heat fluxes and those fluxes predicted from an adaptation of the Coupled Ocean–Atmosphere Response Experiment (COARE),

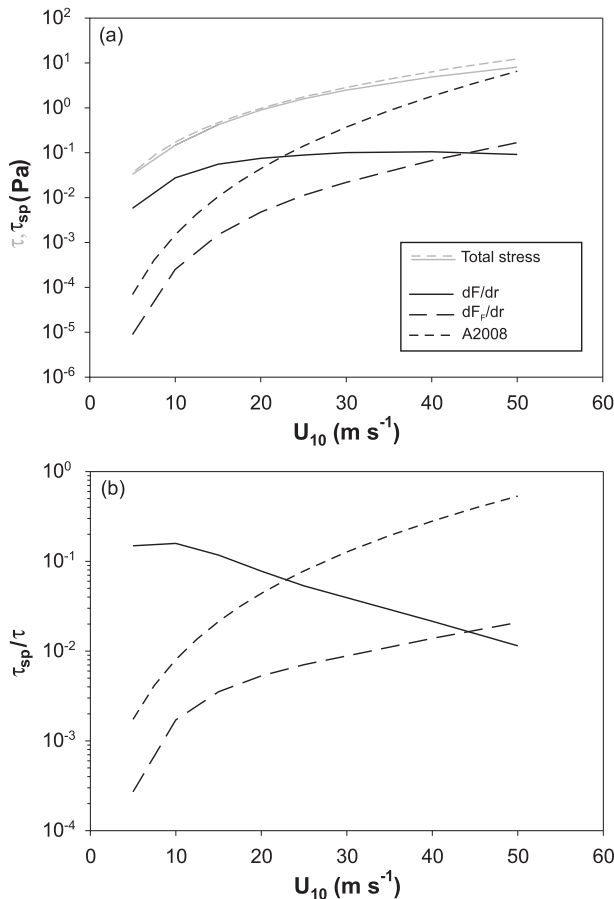


FIG. 1. (a) The spray-mediated stress for the SSGFs of Mueller–Veron (solid) and Fairall et al. (1994; long dashed) along with the spray-mediated stress from A2008 (short dashed). For reference, the total air–sea stress is shown in gray. (b) The fraction of spray-mediated stress relative to total air–sea stress for each SSGF along with results from A2008 for comparison.

version 2.6, algorithm (Fairall et al. 1996). Thus, within the data range at low and moderate wind speeds, the A2008 results are a reasonable representation of observed values. As the magnitude of the heat fluxes become greater, the feedback effects on the atmosphere can no longer be ignored.

### b. Fluxes with feedback

Figure 4 shows how the (Fig. 4a) sensible and (Fig. 4b) latent heat fluxes change with the modeled feedback effects. As expected, the magnitude of the heat fluxes at high wind speeds are smaller with feedback than without feedback for the Fairall et al. (1994) SSGF. At the low and moderate wind speeds, the feedback model also shows an enhanced latent heat flux. The results for the Mueller–Veron SSGF indicate a flux reversal, under certain conditions, which is explored in more detail below.

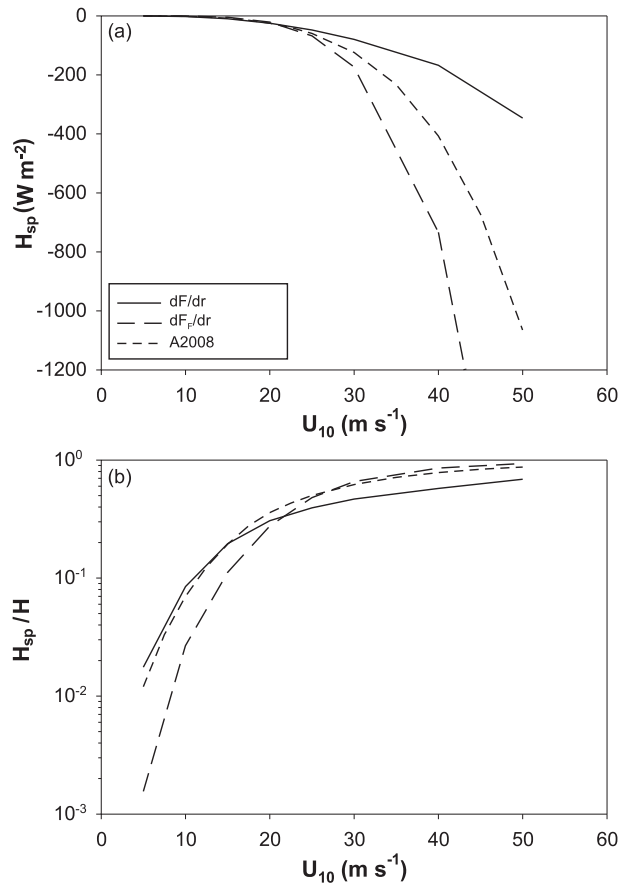


FIG. 2. The spray-mediated sensible heat flux for SSGFs Mueller–Veron (solid) and Fairall et al. (1994; long dashed) along with the spray-mediated sensible heat flux from A2008 (short dashed). (b) The fraction of spray-mediated sensible heat flux relative to total air–sea sensible heat flux for each SSGF along with results from A2008 for comparison.

The feedback behavior can be seen more clearly in Fig. 5, which shows the ratio of the sensible and latent heat fluxes with and without feedback. Coincidentally, the coefficient for the latent heat flux [ $\beta$  here,  $\alpha = 1.5$  in Andreas et al. (2008)] is above one at moderate wind speeds for the Fairall et al. (1994) SSGF. The coefficient for sensible heat remains close to one at low and moderate wind speeds. At high wind speeds, both coefficients decrease to just under 0.6 by  $50 m s^{-1}$ . At low and moderate wind speeds, the coefficients for the Mueller–Veron SSGF are negative, and they increase to roughly one by  $50 m s^{-1}$ . It is worth pointing out here that the fraction of the heat fluxes carried by spray at  $50 m s^{-1}$  for the Mueller–Veron SSGF is about the same as the fraction at  $30 m s^{-1}$  for the Fairall et al. (1994) SSGF. In both cases, the feedback coefficients are close to one. This suggests that the feedback coefficients could decrease again for the Mueller–Veron SSGF at wind speeds above  $50 m s^{-1}$ .

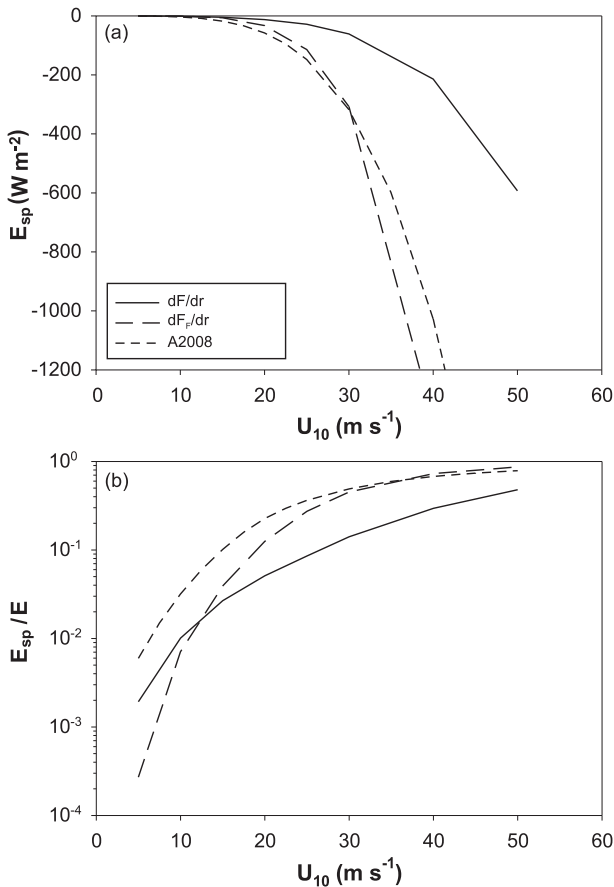


FIG. 3. As in Fig. 2, but for latent heat flux.

Although the behavior may seem rather counterintuitive at first, results presented in Part I show that the behavior of the small and large drops were quite different. The Mueller–Veron SSGF estimates a great deal more large drops, especially at the low wind speeds. As the wind forcing increases, the Mueller–Veron SSGF shifts to smaller and smaller drops, while larger drops stay suspended longer and exchange more with the atmosphere. Consequently, the maximum effect of the large drops relative to small ones occurs at the intermediate wind speeds.

Figures 6 shows the spectral sensible and latent heat fluxes for both SSGFs as a function of the radius. Figures 6a and 6c show the sensible and latent heat fluxes for the Mueller–Veron SSGF, respectively. The smaller drops with feedback carry a greater magnitude of both heat fluxes, while the largest drops carry a flux of the opposite sign. Overall, the largest drops determine the direction of the flux at low and moderate wind speeds. Net fluxes of opposite signs were also found in the Lagrangian results of Part I (see Fig. 11d in Part I). This behavior is exacerbated by the feedback model

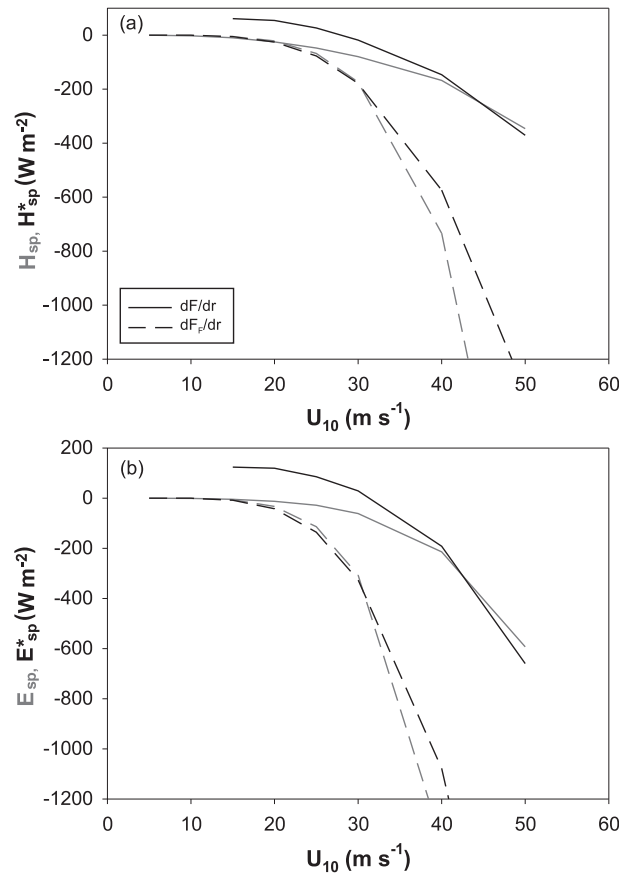


FIG. 4. The spray-mediated (a) sensible and (b) latent heat fluxes for SSGFs Mueller–Veron (solid) and Fairall et al. (1994; long dashed) with feedback effects. For reference, the fluxes without feedback (reported from Figs. 2 to 3) are also shown in gray.

parameterization, which assumes that the largest drops are affected by conditions closer to the surface than the smaller drops because they disperse to a lesser extent within the boundary layer and remain closer to their starting height near the surface.

The feedback of all the drops affects the profiles, which in turn affect drops of all sizes. So the net (sensible and latent) heat flux of the entire distribution near the surface is what determines the profiles there (and consequently even the spectral fluxes). So while we are plotting the spectral fluxes with feedback, the direction will depend on the integrated, net flux of the entire distribution. The large drops have a different net heat flux than the smaller ones. So if the large drops win out (based on the distribution), the net spray-mediated heat flux is different. And that net flux is what will determine even the spectral fluxes.

Figures 6b and 6d show the sensible and latent heat fluxes, respectively, for the Fairall et al. (1994) SSGF. These results are more intuitive; when the magnitude of

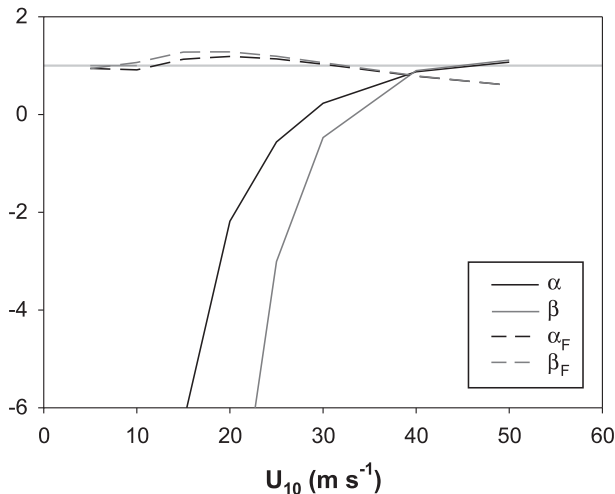


FIG. 5. The feedback coefficients for sensible and latent heat fluxes with Mueller–Veron SSGF (black and gray, respectively) and with Fairall et al. (1994; long dashed).

the total fluxes without feedback becomes significant, the fluxes with feedback become smaller. As seen previously in Figs. 3 and 4, the fluxes are slightly enhanced with feedback at the lower wind speeds.

### c. Profiles with feedback

The spray-mediated fluxes not only contribute to the total effective air–sea fluxes, but because of the different behavior and trajectories for drops of various sizes, they also modify the vertical profiles of momentum, water vapor, and temperature in some unexpected ways. Figure 7 shows how the mean vertical profiles of wind speed, specific humidity, and potential temperature are influenced by the presence of spray and illustrates these vertical profiles with and without feedback effects from spray as well as the differences between the profiles with and without spray present. Because the spray-mediated stress is small relative to the total air–sea momentum flux, the wind profiles are only slightly modified for both SSGFs at both wind speeds shown here.

Because of the significant mass transfer from the evaporation of drops, the vertical profiles of specific humidity show noticeable feedback effects from sea spray. Intuitively, we expect additional water vapor close to the surface where the drops are evaporating. The results shown in Figs. 7c and 7d confirm that expectation. If the 10-m height value is held constant (as is done here), the presence of evaporating spray drops could translate to less water vapor farther above the surface, well above the

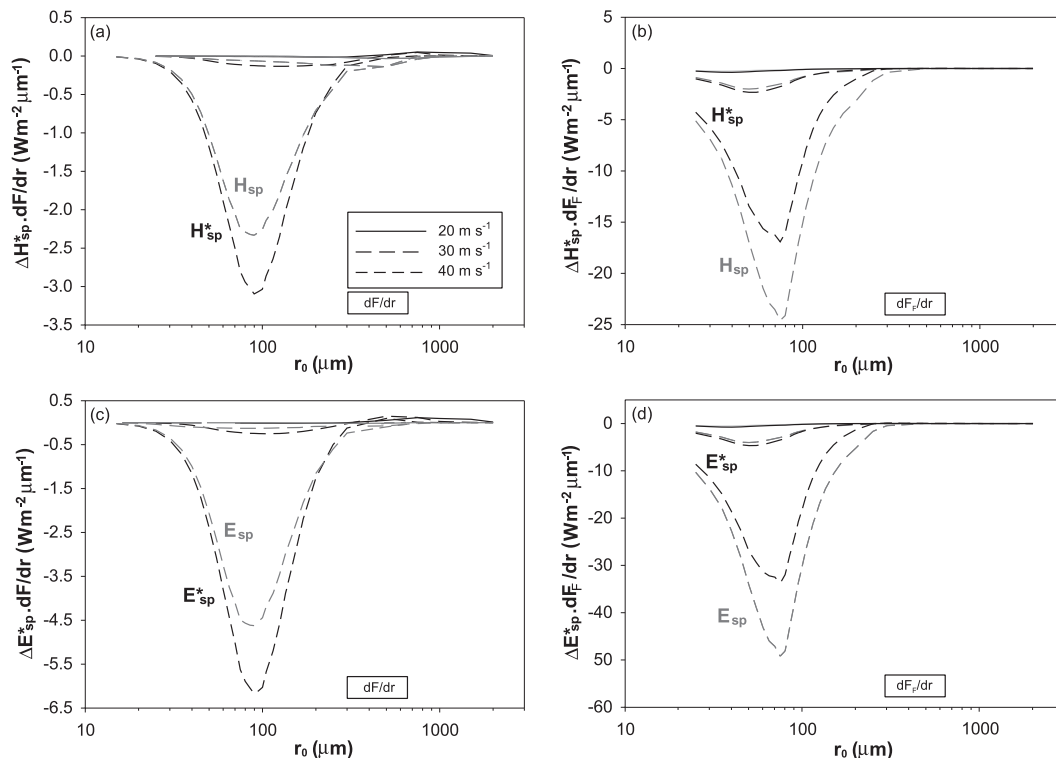


FIG. 6. The spectral sensible heat flux for SSGFs (a) Mueller–Veron and (b) Fairall et al. (1994) and the spectral latent heat flux for SSGFs (c) Mueller–Veron and (d) Fairall et al. (1994) with feedback (black) and without feedback (gray) for 10-m wind speeds of 20 (solid), 30 (long dashed), and 40  $\text{m s}^{-1}$  (short dashed).

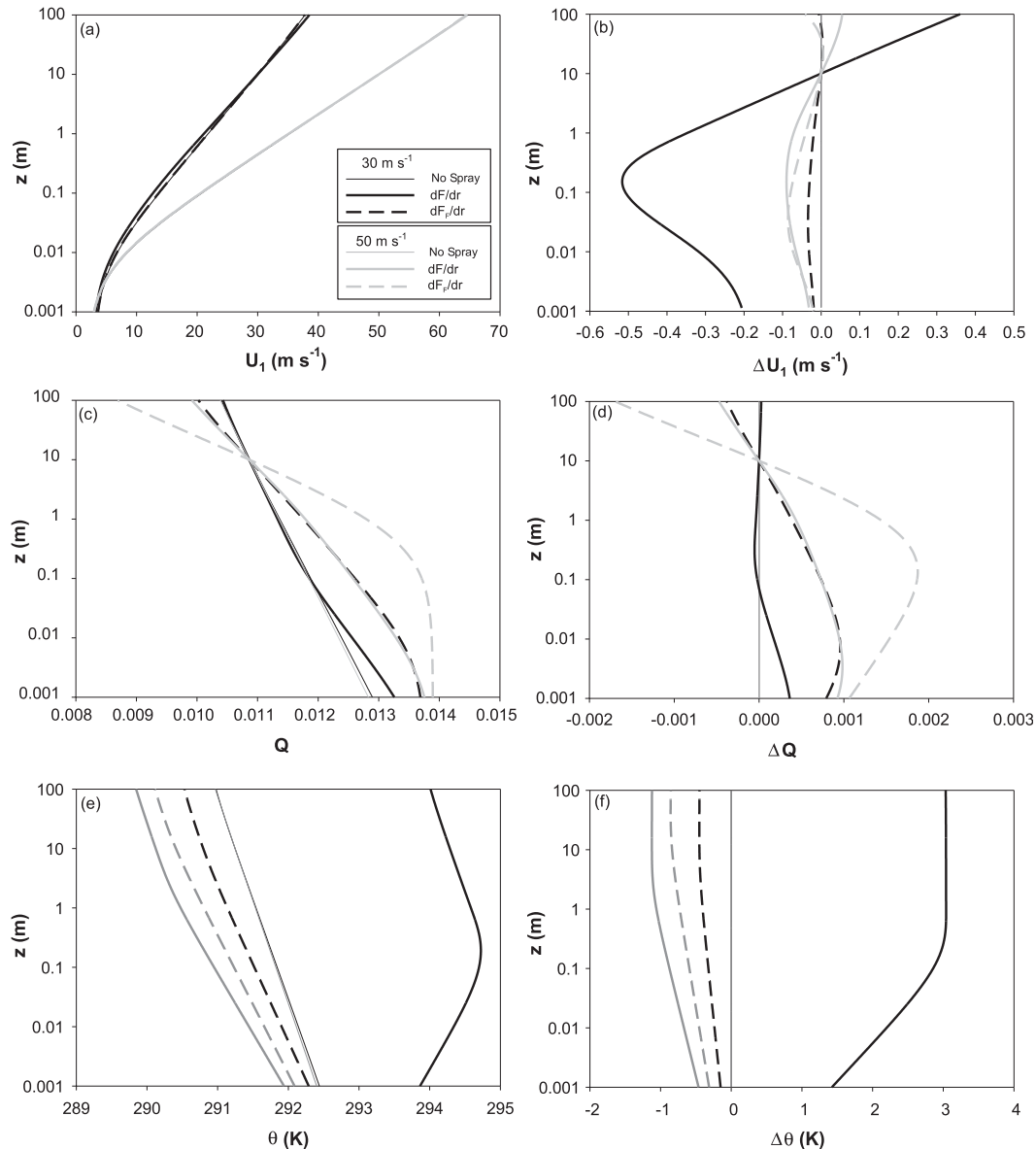


FIG. 7. The vertical profiles of the mean (a) wind speed, (c) specific humidity, and (e) potential temperature at 10-m wind speeds of 30 (black) and 50  $\text{m s}^{-1}$  (gray) without spray (thin lines; these often overlap) and with SSGFs Mueller–Veron (solid) and Fairall et al. (1994; long dashed). The differences between the mean profiles with spray and without spray for (b) wind speed, (d) specific humidity, and (f) potential temperature are also shown.

layer of sea spray drops. Interestingly, the vertical profiles of specific humidity are about the same for the Mueller and Veron SSGF at 50  $\text{m s}^{-1}$  and the Fairall et al. (1994) SSGF at 30  $\text{m s}^{-1}$ , however coincidental.

The presence of spray seems to have the most impact on the vertical profiles of potential temperature. In fact, the feedback effects from spray on the near-surface temperature are generally strong enough that the value at 10-m height cannot be held constant as was done for the specific humidity. As can be seen in Figs. 7e and 7f, the drops tend to cool the atmosphere more with

increasing wind speed and with a greater relative number of smaller drops formed. Increased wind forcing suspends the drops for longer, providing more time to cool the atmosphere through latent heat exchange. Curiously, the presence of spray warms the atmosphere for the Mueller–Veron SSGF at 30  $\text{m s}^{-1}$  wind speed. Although this will be explored further below, this result is qualitatively similar to what Bianco et al. (2011) found. Their Fig. 4 shows that as the drop size increases, the effect of the sea spray drops on the atmosphere transitions from cooling to warming. Although the

Mueller–Veron SSGF projects that the mean radius will decrease with increased wind forcing, at  $30 \text{ m s}^{-1}$  the volume mean radius is still larger than that of most conventional SSGFs.

Figure 8 shows the vertical profiles of the spray-mediated heat fluxes (sensible, latent, and net sensible) at three wind speeds, 30, 40, and  $50 \text{ m s}^{-1}$ , for both SSGFs. The maximum magnitude of the sensible and latent heat fluxes increases with increasing wind speed for both SSGFs, and the maximum magnitude of these fluxes is greater for the Fairall et al. (1994) SSGF at all three wind speeds. Because the Mueller–Veron SSGF predicts more large drops relative to small ones (and these drops remain closer to the surface), the spray-mediated fluxes do not extend as far away from the surface. The net heat fluxes follow a similar pattern, but there is a distinct flux reversal at the low wind speeds for the Mueller–Veron SSGF. Again, this is due to its prediction of large drops that carry fluxes of the opposite sign (see Fig. 6 here and Fig. 11d in Part I).

#### d. Transfer coefficients

From the total direct fluxes (interfacial plus spray mediated), the bulk transfer coefficients are defined as

$$C_D = (\tau_{\text{int}} + \tau_{\text{sp}}) / \{\rho [U_1(10) - U_1(0)] |U_1(10) - U_1(0)|\}, \quad (56)$$

$$C_H = (H_{\text{int}} + \alpha H_{\text{sp}}) / \{\rho c_p [\Theta(10) - \Theta(0)] |U_1(10) - U_1(0)|\}, \quad \text{and} \quad (57)$$

$$C_E = (E_{\text{int}} + \beta E_{\text{sp}}) / \{\rho L_v [Q(10) - Q(0)] |U_1(10) - U_1(0)|\}, \quad (58)$$

where  $C_D$ ,  $C_H$ , and  $C_E$  are the drag coefficient, Stanton number, and Dalton number, respectively. The enthalpy transfer coefficient  $C_K$  can be defined in terms of the sensible and latent heat fluxes and the Stanton and Dalton numbers:

$$C_K = (H + E) \left( \frac{H_{\text{int}} + \alpha H_{\text{sp}}}{C_H} + \frac{E_{\text{int}} + \beta E_{\text{sp}}}{C_E} \right)^{-1}. \quad (59)$$

These coefficients are often reported in the literature with the values under neutral stability conditions. The coefficients above could be converted by substituting the 10-m values calculated with the profiles in Eqs. (31)–(33) while keeping the stability functions equal to zero. Except at the lowest wind speeds, the effects of the stability functions are relatively small under the conditions considered here.

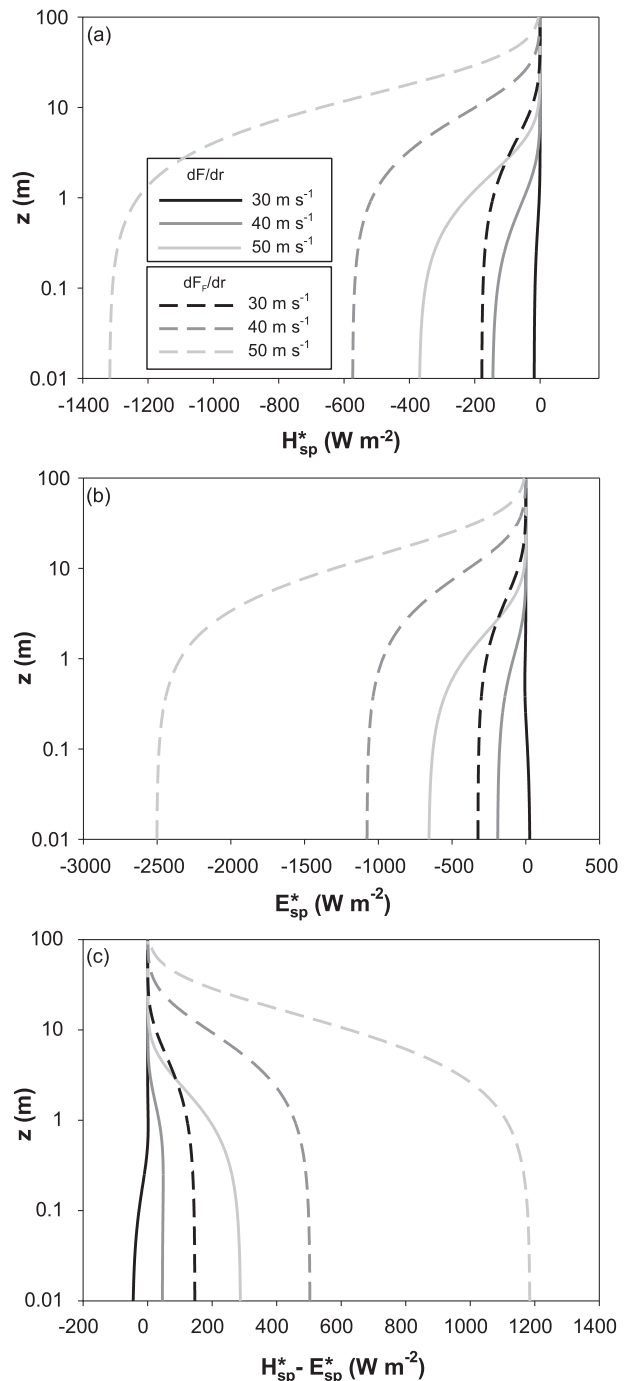


FIG. 8. Vertical profiles of the spray-mediated (a) sensible heat, (b) latent heat, and (c) net heat fluxes with SSGFs Mueller–Veron (solid) and Fairall et al. (1994; long dashed) at 10-m wind speeds 30 (black), 40 (dark gray), and  $50 \text{ m s}^{-1}$  (light gray).

Figure 9 shows the Stanton and Dalton numbers. For reference, the mean and one standard deviation are plotted for both the Coupled Boundary Layer and Air–Sea Transfer (CBLAST; Drennan et al. 2007; Zhang

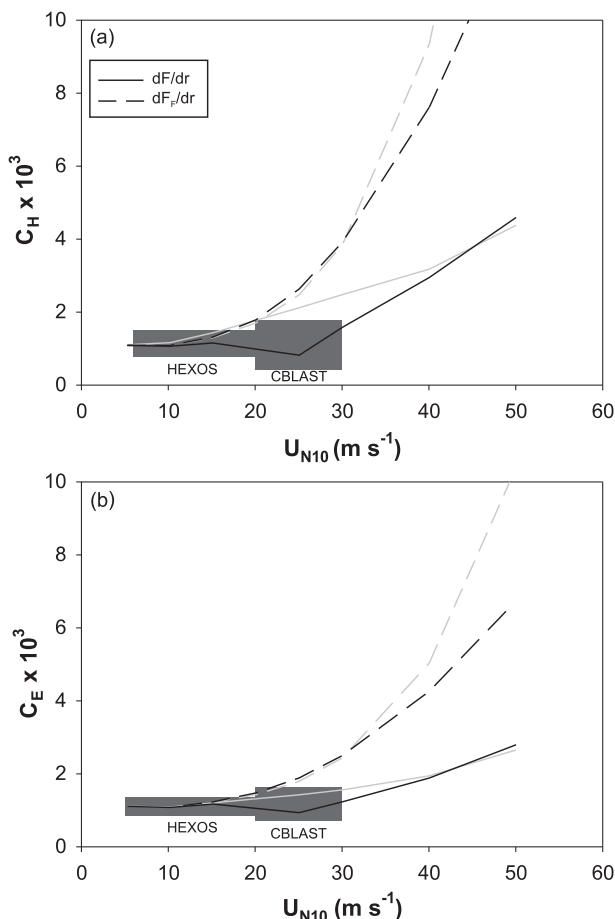


FIG. 9. (a) The Stanton and (b) Dalton numbers for SSGFs Mueller–Veron (solid) and Fairall et al. (1994; long dashed). The empirical ranges from HEXOS and CBLAST experiments are shown in dark gray. The respective transfer coefficients estimated without feedback taken into account are also shown in light gray.

et al. 2008) and Humidity Exchange over the Sea (HEXOS; DeCosmo et al. 1996) experiments. At the lowest wind speeds, all of the scenarios fall within the HEXOS range. Those with the Fairall et al. (1994) SSGF increase rapidly with wind speed and fall outside the HEXOS and CBLAST ranges at the higher wind speeds. The Dalton number of the Mueller–Veron SSGF scenario without feedback falls with the data range for all wind speeds, but the Stanton number does not. When feedback is included, both the Stanton and Dalton numbers remain within the HEXOS and CBLAST data ranges for all wind speeds. Although the CBLAST results do not suggest increasing heat transfer coefficients with wind speed, the model predicts increasing coefficients at the upper end of the data range and beyond.

Figure 10 shows the drag and enthalpy transfer coefficients as a function of 10-m wind speed under neutral conditions. The HEXOS and CBLAST data are included

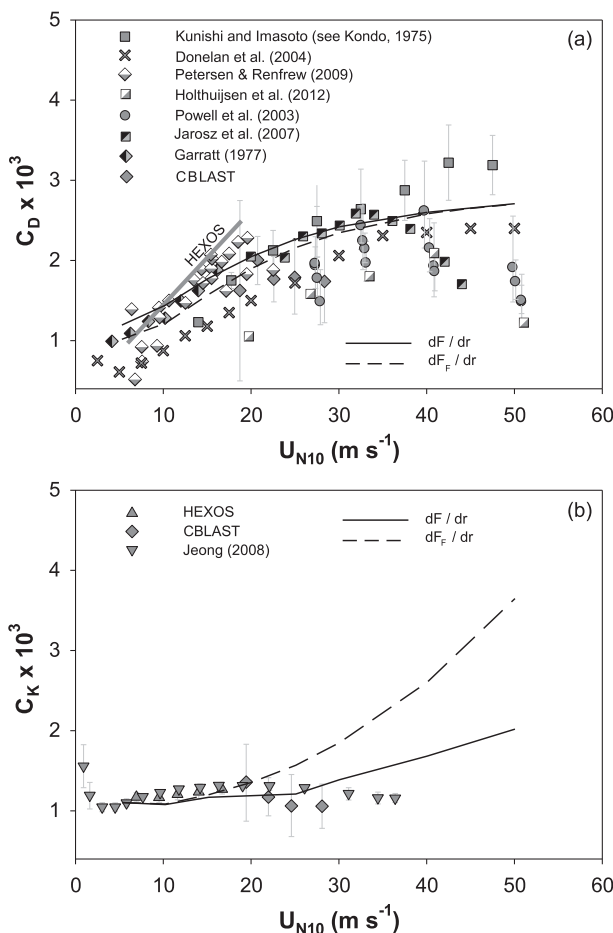


FIG. 10. (a) The drag and (b) enthalpy coefficients for SSGFs Mueller–Veron (solid) and Fairall et al. (1994; long dashed) with feedback along with results from HEXOS (gray line; upward triangles), Donelan et al. (2004; crosses), Kunishi and Imasoto (squares), CBLAST (diamonds), Powell et al. (2003; circles), Jeong (2008; downward triangles), Petersen and Renfrew (2009; half gray diamonds), Holthuijzen et al. (2012; half gray squares), Jarosz et al. (2007; half back squares), and Garratt (1977; half back diamonds).

for reference, as are the drag coefficients from Donelan et al. (2004), Powell et al. (2003), Kondo (1975), Petersen and Renfrew (2009), Jarosz et al. (2007), Garratt (1977), and Holthuijzen et al. (2012) and enthalpy coefficients from Jeong (2008). Except at the low wind speeds, the drag coefficient for both cases are essentially the same and fall within the available data ranges, though they appear to be slightly higher than most datasets at the highest wind speeds. The enthalpy transfer coefficients agree fairly well with the data up to  $20 \text{ m s}^{-1}$ . At wind speeds above that, the scenarios with the Fairall et al. (1994) SSGF increase rapidly and depart from both the data and the scenarios with the Mueller–Veron SSGF. The latter scenarios agree with the data surprisingly well. Even the scenarios with the Fairall et al. (1994)

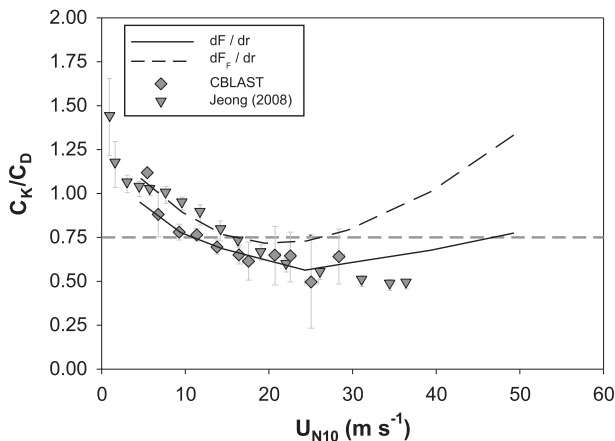


FIG. 11. The ratio of enthalpy and drag coefficients for SSGFs Mueller–Veron (solid) and Fairall et al. (1994; long dashed) with feedback. Also shown are the results from HEXOS and CBLAST (diamonds) and Jeong (2008, downward triangles).

SSGF find lower enthalpy coefficients at high wind speeds than those in Andreas (2011), as plotted in his Fig. 2 for a sea surface temperature of 20°C. While his coefficients are for neutral stability conditions, our scenarios present slightly unstable conditions in which the 10-m air temperature is 2°C cooler than the sea surface.

Looking at the ratio of the enthalpy transfer coefficient and the drag coefficient in Fig. 11, we find that the scenario with the Fairall et al. (1994) SSGF agrees with the upper limit of the available data at low wind speed and barely stays within the CBLAST data range at higher wind speeds, where the model estimates for both coefficients are higher than the data suggest. The ratio estimated using the Mueller–Veron SSGF agrees rather well with the available data over the entire data range. We note, however, that both scenarios suggest that the ratio of the enthalpy transfer coefficient and the drag coefficient increases again at higher wind speeds. Data are sparse in that wind speed range, so it is difficult to confirm or refute this behavior. The Jeong (2008) data presented are the “modified” ratio, for which the drag coefficient is assumed to be the value given by the Tropical Ocean Global Atmosphere Coupled Ocean–Atmosphere Response Experiment (TOGA COARE) 3.0 algorithm (Fairall et al. 2003; Grachev et al. 2000) based on Businger et al. (1971) and Beljaars and Holtslag (1991).

## 5. Discussion and conclusions

In the cases without accounting for feedback effects, we find a reasonable upper bound for the spray-mediated heat fluxes, but the ratio of the enthalpy and drag coefficients at high wind speeds remains an open

question. Empirical observations suggest that the ratio remains below the Emanuel threshold of 0.75 at moderate to high wind speeds. The results presented here provide a potential explanation: at low-to-moderate wind speeds the drag coefficient increases, while the enthalpy coefficient remains roughly constant; at higher wind speeds, the drag coefficient remains roughly constant, while the enthalpy coefficient increases. Because of feedback effects and the saturation of spray, this increase in the enthalpy coefficient presumably does not increase indefinitely. Nevertheless, empirical data do extend to sufficiently high wind speeds to rule out the possibility of an increased enthalpy to drag coefficient ratio. Further investigation into both coefficients, particularly the enthalpy coefficient, at high wind speeds is critical.

When considering feedback effects, we find that the heat fluxes from traditional SSGFs with relatively more of the smaller drops behave as expected from conventional wisdom. As the spray-mediated heat fluxes constitute a larger fraction of the total heat fluxes, feedback effects reduce the efficiency of spray-mediated fluxes and mitigate an increasing fraction of the fluxes without feedback. There is an exception at low-to-moderate wind speeds where the feedback effects actually enhance the spray-mediated fluxes slightly. The same trend cannot describe the behavior for SSGFs with relatively more of the larger drops, however. Although there is no simple rule of thumb, the trend seems to be nearly opposite.

The spray-mediated stress remains a small fraction of the total stress for all conditions except those with a large number of the largest drop sizes. The range of wind speed conditions for which feedback needs to be considered is uncertain and tied directly to the size distribution of the drops.

The results presented above underscore size distribution as another critical factor in need of further investigation. In that regard, we note here that the SSGF of Mueller and Veron (2009c) is substantially lower than that of Fairall et al. (1994), at least in high winds and for open-ocean conditions. The lack of spray data in high winds continues to prevent better parameterizations. Still, the agreement with the available experimental results of Figs. 10 and 11 is encouraging. Recently Veron et al. (2012) found more of the largest drops at high wind speeds than either of the SSGFs considered here. Based on the results of this model, more of the largest drops would have the effect of decreasing the enthalpy to drag coefficient ratio further through two pathways. The large drops hold sufficient mass and momentum to increase the effective drag coefficient significantly. The heat flux reversal found within the large drop regime

would also suggest lower enthalpy transfer. In combination, both of these effects from more large drops would lead to a lower enthalpy to drag coefficient ratio.

This study calls for further validation of the simplified feedback model, which we hope will agree with subsequent, full simulations of the feedback effects. As noted in Part I, another future consideration is the impact of relative humidity, which previous studies (e.g., Innocentini and Goncalves 2010; Shpund et al. 2012) have found to be an important parameter for feedback effects. In addition, we suggest that the role of large drops is neither fully understood nor accounted for and that some effort should be put toward investigating their potential presence and effects on the multiple fluxes at high wind speeds.

*Acknowledgments.* We thank Ed Andreas, Kristina Katsaros, and an anonymous reviewer for comments that helped improve the paper. This research was supported by Grants OCE-0850663 and OCE-0748767 from the National Science Foundation (NSF) and Grant N00014-05-1-0609 from the Office of Naval Research (ONR).

#### REFERENCES

- Andreas, E. L., 1989: Thermal and size evolution of sea spray droplets. U. S. Army Corp of Engineers Cold Regions Research and Engineering Laboratory CRELL Rep. 89-11, 47 pp.
- , 1990: Time constants for the evolution of sea spray droplets. *Tellus*, **42B**, 481–497, doi:10.1034/j.1600-0889.1990.t01-3-00007.x.
- , 1992: Sea spray and the turbulent air-sea heat fluxes. *J. Geophys. Res.*, **97**, 11 429–11 441, doi:10.1029/92JC00876.
- , 2002: A review of the sea spray generation function for the open ocean. *Atmosphere-Ocean Interactions*, W. A. Perrie, Ed., Advances in Fluid Mechanics, Vol. 1, WIT Press, 1–46.
- , 2004: Spray stress revisited. *J. Phys. Oceanogr.*, **34**, 1429–1440, doi:10.1175/1520-0485(2004)034<1429:SSR>2.0.CO;2.
- , 2011: Fallacies of the enthalpy transfer coefficient over the ocean in high winds. *J. Atmos. Sci.*, **68**, 1435–1445, doi:10.1175/2011JAS3714.1.
- , and J. DeCosmo, 1999: Sea spray production and influence on air-sea heat and moisture fluxes over the open ocean. *Air-Sea Exchange: Physics, Chemistry and Dynamics*, G. L. Geernaert, Ed., Kluwer, 327–362, doi:10.1007/978-94-015-9291-8\_13.
- , and K. A. Emanuel, 2001: Effects of sea spray on tropical cyclone intensity. *J. Atmos. Sci.*, **58**, 3741–3751, doi:10.1175/1520-0469(2001)058<3741:E0SSOT>2.0.CO;2.
- , P. O. G. Persson, and J. E. Hare, 2008: A bulk turbulent air-sea flux algorithm for high-wind, spray conditions. *J. Phys. Oceanogr.*, **38**, 1581–1596, doi:10.1175/2007JPO3813.1.
- Bao, J.-W., C. W. Fairall, S. A. Michelson, and L. Bianco, 2011: Parameterizations of sea-spray impact on the air-sea momentum and heat fluxes. *Mon. Wea. Rev.*, **139**, 3781–3797, doi:10.1175/MWR-D-11-00007.1.
- Barenblatt, G. I., A. J. Chorin, and V. M. Prostokishin, 2005: A note concerning the Lighthill “sandwich model” of tropical cyclones. *Proc. Natl. Acad. Sci. USA*, **102**, 11 148–11 150, doi:10.1073/pnas.0505209102.
- Beard, K. V., and H. R. Pruppacher, 1971: A wind tunnel investigation of rate of evaporation of small water drops falling at terminal velocity in air. *J. Atmos. Sci.*, **28**, 1455–1464, doi:10.1175/1520-0469(1971)028<1455:AWTIOT>2.0.CO;2.
- Beljaars, A. C. M., and A. A. M. Holtslag, 1991: Flux parameterization over land surfaces for atmospheric models. *J. Appl. Meteor.*, **30**, 327–341, doi:10.1175/1520-0450(1991)030<0327:FPOLSF>2.0.CO;2.
- Bianco, L., J. W. Bao, C. W. Fairall, and S. A. Michelson, 2011: Impact of sea-spray on the atmospheric surface layer. *Boundary Layer Meteor.*, **140**, 361–381, doi:10.1007/s10546-011-9617-1.
- Black, P. G., and Coauthors, 2007: Air-sea exchange in hurricanes: Synthesis of observations from the coupled boundary layer air-sea transfer experiment. *Bull. Amer. Meteor. Soc.*, **88**, 357–374, doi:10.1175/BAMS-88-3-357.
- Blanchard, D. C., and A. H. Woodcock, 1957: Bubble formation and modification in the sea and its meteorological significance. *Tellus*, **9**, 145–158, doi:10.1111/j.2153-3490.1957.tb01867.x.
- Bryan, G. H., and R. Rotunno, 2009a: Evaluation of an analytical model for the maximum intensity of tropical cyclones. *J. Atmos. Sci.*, **66**, 3042–3060, doi:10.1175/2009JAS3038.1.
- , and —, 2009b: The maximum intensity of tropical cyclones in axisymmetric numerical model simulations. *Mon. Wea. Rev.*, **137**, 1770–1789, doi:10.1175/2008MWR2709.1.
- Businger, J. A., J. C. Wyngaard, Y. Izumi, and E. F. Bradley, 1971: Flux-profile relationships in atmospheric surface layer. *J. Atmos. Sci.*, **28**, 181–189, doi:10.1175/1520-0469(1971)028<0181:FPRITA>2.0.CO;2.
- Bye, J. A. T., and A. D. Jenkins, 2006: Drag coefficient reduction at very high wind speeds. *J. Geophys. Res.*, **111**, C03024, doi:10.1029/2005JC003114.
- Clift, R., and W. H. Gauvin, 1970: The motion of particles in turbulent gas streams. *Proc. Chemeca '70*, Vol. 1, 14–28.
- , J. R. Grace, and M. E. Weber, 1978: *Bubbles, Drops, and Particles*. Academic Press, 380 pp.
- DeCosmo, J., K. B. Katsaros, S. D. Smith, R. J. Anderson, W. A. Oost, K. Bumke, and H. Chadwick, 1996: Air-sea exchange of water vapor and sensible heat: The Humidity Exchange over the Sea (HEXOS) results. *J. Geophys. Res.*, **101**, 12 001–12 016, doi:10.1029/95JC03796.
- Donelan, M. A., B. K. Haus, N. Reul, W. J. Plant, M. Stiassnie, H. C. Graber, O. B. Brown, and E. S. Saltzman, 2004: On the limiting aerodynamic roughness of the ocean in very strong winds. *Geophys. Res. Lett.*, **31**, L18306, doi:10.1029/2004GL019460.
- Drennan, W. M., J. A. Zhang, J. R. French, C. McCormick, and P. G. Black, 2007: Turbulent fluxes in the hurricane boundary layer. Part II: Latent heat flux. *J. Atmos. Sci.*, **64**, 1103–1115, doi:10.1175/JAS3889.1.
- Edson, J. B., and C. Fairall, 1998: Similarity relationships in the marine surface layer. *J. Atmos. Sci.*, **55**, 2311–2328, doi:10.1175/1520-0469(1998)055<2311:SRITMA>2.0.CO;2.
- , S. Anquetin, P. G. Mestayer, and J. F. Sini, 1996: Spray droplet modeling: 2. An interactive Eulerian-Lagrangian model of evaporating spray droplets. *J. Geophys. Res.*, **101**, 1279–1293, doi:10.1029/95JC03280.
- Elfouhaily, T., B. Chapron, K. Katsaros, and D. Vandemark, 1997: A unified directional spectrum for long and short wind-driven waves. *J. Geophys. Res.*, **102**, 15 781–15 796, doi:10.1029/97JC00467.
- Emanuel, K. A., 1986: An air-sea theory for tropical cyclones. Part I: Steady-state maintenance. *J. Atmos. Sci.*, **43**, 585–604, doi:10.1175/1520-0469(1986)043<0585:AASITF>2.0.CO;2.

- , 1995: Sensitivity of tropical cyclones to surface exchange coefficients and a revised steady-state model incorporating eye dynamics. *J. Atmos. Sci.*, **52**, 3969–3976, doi:10.1175/1520-0469(1995)052<3969:SOTCTS>2.0.CO;2.
- Fairall, C. W., J. D. Kepert, and G. J. Holland, 1994: The effect of sea spray on surface energy transports over the ocean. *Global Atmos. Ocean Syst.*, **2**, 121–142.
- , E. F. Bradley, D. P. Rogers, J. B. Edson, and G. S. Young, 1996: Bulk parameterization of air-sea fluxes for tropical ocean-global atmosphere coupled-ocean atmosphere response experiment. *J. Geophys. Res.*, **101**, 3747–3764, doi:10.1029/95JC03205.
- , —, J. E. Hare, A. A. Grachev, and J. B. Edson, 2003: Bulk parameterization of air-sea fluxes: Updates and verification for the COARE algorithm. *J. Climate*, **16**, 571–591, doi:10.1175/1520-0442(2003)016<0571:BPOASF>2.0.CO;2.
- Fitzgerald, J. W., 1975: Approximation formulas for the equilibrium size of an aerosol particle as a function of its dry size and composition and the ambient relative humidity. *J. Appl. Meteor.*, **14**, 1044–1049, doi:10.1175/1520-0450(1975)014<1044:AFFTES>2.0.CO;2.
- French, J. R., W. M. Drennan, J. A. Zhang, and P. G. Black, 2007: Turbulent fluxes in the hurricane boundary layer. Part I: Momentum flux. *J. Atmos. Sci.*, **64**, 1089–1102, doi:10.1175/JAS3887.1.
- Garratt, J. R., 1977: Review of drag coefficients over oceans and continents. *Mon. Wea. Rev.*, **105**, 915–929, doi:10.1175/1520-0493(1977)105<0915:RODCOO>2.0.CO;2.
- Grachev, A. A., C. W. Fairall, and E. F. Bradley, 2000: Convective profile constants revisited. *Bound.-Layer Meteor.*, **94**, 495–515, doi:10.1023/A:1002452529672.
- Haus, B. K., D. Jeong, M. A. Donelan, J. A. Zhang, and I. Savelyev, 2010: Relative rates of sea-air heat transfer and frictional drag in very high winds. *Geophys. Res. Lett.*, **37**, L07802, doi:10.1029/2009GL042206.
- Hinze, J. O., 1955: Fundamentals of the hydrodynamic mechanism of splitting in dispersion processes. *AIChE J.*, **1**, 289–295, doi:10.1002/aic.690010303.
- Holthuijsen, L. H., M. D. Powell, and J. D. Pietrzak, 2012: Wind and waves in extreme hurricanes. *J. Geophys. Res.*, **117**, C09003, doi:10.1029/2012JC009783.
- Innocentini, V., and I. A. Gonalves, 2010: The impact of spume droplets and wave stress parameterizations on simulated near-surface maritime wind and temperature. *J. Phys. Oceanogr.*, **40**, 1373–1389, doi:10.1175/2010JPO4349.1.
- Jarosz, E., D. A. Mitchell, D. W. Wang, and W. J. Teague, 2007: Bottom up determination of air-sea momentum exchange under a major tropical cyclone. *Science*, **315**, 1707–1709, doi:10.1126/science.1136466.
- Jeong, D., 2008: Laboratory measurements of the moist enthalpy transfer coefficient. M.S. thesis, Rosenstiel School of Marine and Atmospheric Science, University of Miami, 63 pp.
- Kondo, J., 1975: Air-sea bulk transfer coefficients in diabatic conditions. *Bound.-Layer Meteor.*, **9**, 91–112, doi:10.1007/BF00232256.
- Kudryavtsev, V. N., 2006: On effect of sea drops on atmospheric boundary layer. *J. Geophys. Res.*, **111**, C07020, doi:10.1029/2005JC002970.
- , and V. K. Makin, 2007: Aerodynamic roughness of the sea surface at high winds. *Bound.-Layer Meteor.*, **125**, 289–303, doi:10.1007/s10546-007-9184-7.
- , and —, 2011: Impact of ocean spray on the dynamics of the marine atmospheric boundary layer. *Bound.-Layer Meteor.*, **140**, 383–410, doi:10.1007/s10546-011-9624-2.
- Lighthill, J., 1999: Ocean spray and the thermodynamics of tropical cyclones. *J. Eng. Math.*, **35**, 11–42, doi:10.1023/A:1004383430896.
- Lumley, J. L., and H. A. Panofsky, 1964: *The Structure of Atmospheric Turbulence*. J. Wiley and Sons, 229 pp.
- Makin, V. K., and V. N. Kudryavtsev, 1999: Coupled sea surface-atmosphere model: 1. Wind over waves coupling. *J. Geophys. Res.*, **104**, 7613–7624, doi:10.1029/1999JC900006.
- Meirink, J., 2002: The role of wind-waves and sea spray on air-sea interaction. Ph.D. dissertation, Technische Universiteit Delft, 161 pp.
- Mestayer, P. G., and Coauthors, 1990: CLUSE simulations of the vapor flux modification by droplet evaporation. Modelling the fate and influence of marine spray, Marine Sciences Institute, University of Connecticut, Whitecap Rep. 7, 100–105.
- Monahan, E. C., and I. O’Muircheartaigh, 1980: Optimal power-law description of oceanic whitecap coverage dependence on wind speed. *J. Phys. Oceanogr.*, **10**, 2094–2099, doi:10.1175/1520-0485(1980)010<2094:OPLDOO>2.0.CO;2.
- Monin, A. S., and A. M. Obukhov, 1954: Basic laws of turbulent mixing in the surface layer of the atmosphere. *Tr. Geofiz. Inst. Akad. Nauk SSSR*, **24**, 163–187.
- Mueller, J. A., and F. Veron, 2009a: A Lagrangian stochastic model for heavy particle dispersion in the atmospheric marine boundary layer. *Bound.-Layer Meteor.*, **130**, 229–247, doi:10.1007/s10546-008-9340-8.
- , and —, 2009b: Nonlinear formulation of the bulk surface stress over breaking waves: Feedback mechanisms from air-flow separation. *Bound.-Layer Meteor.*, **130**, 117–134, doi:10.1007/s10546-008-9334-6.
- , and —, 2009c: A sea state-dependent spume generation function. *J. Phys. Oceanogr.*, **39**, 2363–2372, doi:10.1175/2009JPO4113.1.
- , and —, 2010a: A Lagrangian stochastic model for sea-spray evaporation in the atmospheric marine boundary layer. *Bound.-Layer Meteor.*, **137**, 135–152, doi:10.1007/s10546-010-9520-1.
- , and —, 2010b: Bulk formulation of the heat and water vapor fluxes at the air-sea interface, including nonmolecular contributions. *J. Atmos. Sci.*, **67**, 234–247, doi:10.1175/2009JAS3061.1.
- , and —, 2014: Impact of sea spray on air-sea fluxes. Part I: Results from stochastic simulations of sea spray drops over the ocean. *J. Phys. Oceanogr.*, **44**, 2817–2834, doi:10.1175/JPO-D-13-0245.1.
- Obukhov, A. M., 1946: Turbulence in an atmosphere with non-uniform temperature. *Tr. Inst. Teor. Geofiz. Nauk SSSR*, **1**, 95–115.
- Petersen, G. N., and I. A. Renfrew, 2009: Aircraft-based observations of air-sea fluxes over Denmark Strait and the Irminger Sea during high wind speed conditions. *Quart. J. Roy. Meteor. Soc.*, **135**, 2030–2045, doi:10.1002/qj.355.
- Powell, M. D., P. J. Vickery, and T. A. Reinhold, 2003: Reduced drag coefficient for high wind speeds in tropical cyclones. *Nature*, **422**, 279–283, doi:10.1038/nature01481.
- Pruppacher, H. R., and J. D. Klett, 1978: *Microphysics of Clouds and Precipitation*. D. Riedel, 714 pp.
- Raudviki, A. J., 1976: *Loose Boundary Hydraulics*. Pergamon Press, 397 pp.
- Richter, D. H., and P. P. Sullivan, 2013: Sea surface drag and the role of spray. *Geophys. Res. Lett.*, **40**, 656–660, doi:10.1002/grl.50163.

- Shpund, J., J. A. Zhang, M. Pinsky, and A. Khain, 2012: Microphysical structure of the marine boundary layer under strong wind and spray formation as seen from simulations using a 2D explicit microphysical model. Part II: The role of sea spray. *J. Atmos. Sci.*, **69**, 3501–3514, doi:[10.1175/JAS-D-11-0281.1](https://doi.org/10.1175/JAS-D-11-0281.1).
- Van Eijk, A. M. J., B. S. Tranchant, and P. G. Mestayer, 2001: SeaCluse: Numerical simulation of evaporating sea spray droplets. *J. Geophys. Res.*, **106**, 2573–2588, doi:[10.1029/2000JC000377](https://doi.org/10.1029/2000JC000377).
- Veron, F., C. Hopkins, E. Harrison, and J. Mueller, 2012: Sea spray spume droplet production in high wind speeds. *Geophys. Res. Lett.*, **39**, L16602, doi:[10.1029/2012GL052603](https://doi.org/10.1029/2012GL052603).
- Wyngaard, J. C., 1973: On surface layer turbulence. *Workshop on Micrometeorology*, D. A. Haugen, Ed., Amer. Meteor. Soc., 101–149.
- Zhang, J. A., P. G. Black, J. R. French, and W. M. Drennan, 2008: First direct measurements of enthalpy flux in the hurricane boundary layer: The CBLAST results. *Geophys. Res. Lett.*, **35**, L14813, doi:[10.1029/2008GL034374](https://doi.org/10.1029/2008GL034374).